文章编号: 1001－2060(2010)01－0077－05

一种余热利用相变石蜡储热过程的数值模拟

邹得球[1], 肖 睿[2], 宋文吉[2], 冯自平[2]
(1. 中国科学院研究生院, 北京 100039; 2. 中国科学院广州能源研究所, 广东 广州 510640)

摘 要: 基于一种相变储热石蜡, 考虑熔化过程中液相的自然对流情况, 建立了矩形腔内石蜡熔化过程的数学模型, 并利用该模型进行了数值模拟, 分析了石蜡熔化过程中的温度场变化、流场变化、相界面移动情况。通过采用铝制翅片的方式强化传热, 并分析了翅片位置对该石蜡熔化时间的影响。模拟结果表明, 在 $y=0.1$、$y=5$、$y=10$、$y=15$ mm时, 与不采用翅片相比, 储热时间分别缩短了 43.1%、52.0%、38.3%、22.2%。研究结果对相变储热器的优化设计有一定意义。

关 键 词: 石蜡; 相变; 强化传热; 余热利用; 数值模拟
中图分类号: TK02; O373 文献标识码: A

符号说明

β—液相分数;	t_{ref}—参考温度 /℃;
α—热膨胀系数 /K^{-1};	T_L—相变终点温度 /K;
h—显热比焓 /J·kg^{-1}	ρ—密度 /kg·m^{-3};
ε—小于 0.000 1的数, 防止被 0除;	H—任意时刻的比焓 /J·kg^{-1};
A_{mush}—糊状区域的连续数 (一般值在 $10^4 \sim 10^7$);	μ—动力粘度 /kg·(m·s)$^{-1}$;
h_{ref}—基准比焓 (初始焓值) /J·kg^{-1};	ΔH—潜焓 /J·kg^{-1};
L—相变潜热 /J·kg^{-1};	t—时间 /s;
c_p—定压比热 /J·(kg·K)$^{-1}$;	T—任意时刻的温度 /K;
v—y方向速度 /m·s^{-1};	T_m—初始温度 /K;
	u—x方向速度 /m·s^{-1};
	λ—导热系数 /W·(m·K)$^{-1}$;
	T_s—相变起始点温度 /K;

引 言

石蜡是从石油中提炼出来不同分子量烷烃类的混合物[1], 它具有较高的相变潜热值, 相变过程中无过冷及析出现象, 性能稳定、无毒、无腐蚀性, 因此, 石蜡相变储能材料的研究和使用受到了广泛的重视。虽然石蜡具有上述诸多优点, 但也存在导热系数小的缺点, 所以目前对石蜡类相变材料的研究主要在提高其导热系数方面。为了提高石蜡的导热系数, 强化石蜡的导热, 研究者主要从蓄热设备的改进, 比如采用肋片、添加金属粉末、金属网、石墨等[2~5]。

目前, 国内外对储热石蜡的材料研究, 大多选择相变温度点在 25~60 ℃, 主要用于建筑储能及太阳能储热等方面[6]。事实上, 除了上述热能可以利用之外, 工业上存在大量 100 ℃左右的蒸汽和烟气, 由于工况的不稳定或者排放的间歇性, 当前不能直接利用而排放, 而利用相变材料的相变储能可以解决这种时间、空间不匹配的矛盾, 因而, 寻找合适相变点的相变材料成为利用这部分余热的关键。本实验室在相变蓄冷的研究基础上[7~9], 针对此情况, 进行了大量石蜡类材料的测试, 选取了相变温度合适、潜热值较高的石蜡[10], 图 1为采用差示扫描量热法 (Differential Scanning Calorimetry, 简称 DSC)对石蜡材料测试的曲线 (升温速率 10 ℃/min, 氮气气氛)。由图可知: 该石蜡只有一个吸热峰, 峰值熔化温度为 87 ℃, 相变区间集中在 75~90 ℃, 相变潜热为 203.9 kJ/kg。本研究针对该种石蜡的熔化储热过程进行了数值模拟并对翅片强化传热效果进行了分析。

1 物理模型和数学模型

1.1 物理模型

图 2为物理模型, 从图中可看出, 石蜡填充在矩形腔内, 腔体尺寸为 20 mm×20 mm, 左侧壁为恒温 (373.15 K)壁, 其它各壁面绝热。相变材料为石蜡, 翅片材料为铝, 翅片厚度 0.2 mm, 物性参数如表

收稿日期: 2009－02－23; 修订日期: 2009－09－11
基金项目: 国家自然科学基金—广东联合基金资助项目 (U0634005); 国家 863计划基金资助项目 (2006AA05Z254); 国家自然科学基金资助项目 (50906089)
作者简介: 邹得球 (1981－), 男, 湖南衡阳人, 中国科学院研究生院博士研究生.

1所示。为了分析翅片位置对传热的强化效果，分别模拟了翅片中心线位置：$y=0.1$ mm，$y=5$ mm，$y=10$ mm和 $y=15$ mm 4个位置下石蜡的熔化过程。按照二维非稳态进行计算，并采用以下基本假设：(1)液相石蜡为不可压缩牛顿流体，作层流流动，忽略粘性耗散；(2)满足 Boussinesq假设，即只在浮升力项中考虑流体密度的变化，密度变化仅考虑动量方程中与体积有关的项，此时 $\rho=\rho_{ref}[1-\alpha(t-t_{ref})]$，其余各项中的密度为常数；(3)固相区、液相区作常物性处理，两相区导热系数作线性插值；

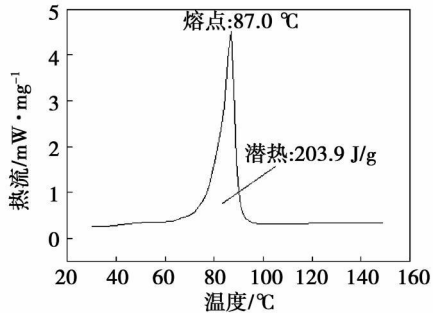

图 1 石蜡熔化过程的 DSC曲线

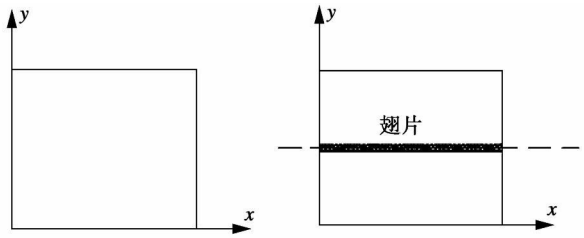

图 2 物理模型

(4)石蜡发生相变的温度范围为 70~95 ℃；(5)石蜡熔化过程中存在固相区、两相区(糊状区)和液相区，把两相区域(部分凝固的区域)看作为多孔介质，每个单元的多孔性在单元中设置相等的流动阻力，对于全凝固的区域，多孔性为 0，液相区多孔性为 1，两相区中多孔性与温度变化成线性关系。

1.2 数学模型

由于相变过程中固液相变界面位置不断移动，使得相变问题具有非线性的特征，除了少数简单的情况外，很难得到该类问题的精确解。因而，基于焓法，采用数值方法求解。焓法是将热焓和温度一起作为待求函数，在整个区域建立一个统一的能量方程，利用数值方法求出焓分布，然后确定两相界面。因此它不需要跟踪界面，无需将固液分开处理，不必分区建立控制方程，其控制方程为：

表 1 石蜡及翅片物性参数

	石蜡	翅片
参考密度 /kg·m⁻³	920	2 719
比热容 /J·(kg·K)⁻¹	2 100	871
固相导热系数 /W·(m·K)⁻¹	0.45	202.4
液相导热系数 /W·(m·K)⁻¹	0.2	—
相变起始点 /K	343.15	—
相变终点 /K	368.15	—
熔化潜热 /J·kg⁻¹	203 900	—
动力粘度 /kg·(m·s)⁻¹	0.01	—
热膨胀系数 /K⁻¹	8.5×10^{-4}	—

连续方程：

$$\frac{\partial\rho}{\partial t}+\frac{\partial(\rho u)}{\partial x}+\frac{\partial(\rho v)}{\partial y}=0 \tag{1}$$

动量方程：

$$\rho\left(\frac{\partial u}{\partial t}+u\frac{\partial u}{\partial x}+v\frac{\partial u}{\partial y}\right)=\mu\left(\frac{\partial^2 u}{\partial x^2}+\frac{\partial^2 u}{\partial y^2}\right)-\frac{\partial p}{\partial x}+S_u \tag{2}$$

$$\rho\left(\frac{\partial v}{\partial t}+u\frac{\partial v}{\partial x}+v\frac{\partial v}{\partial y}\right)=\mu\left(\frac{\partial^2 v}{\partial x^2}+\frac{\partial^2 v}{\partial y^2}\right)-\frac{\partial p}{\partial y}+S_v \tag{3}$$

$$S_u=\frac{(1-\beta)^2}{(\beta^3+\varepsilon)}A_{mush}u \tag{4}$$

$$S_v=\frac{(1-\beta)^2}{(\beta^3+\varepsilon)}A_{mush}v+\rho_{ref}g\alpha(t-t_{ref}) \tag{5}$$

能量方程：

$$\rho\left(\frac{\partial H}{\partial t}+u\frac{\partial H}{\partial x}+v\frac{\partial H}{\partial y}\right)=\frac{k}{c_p}\left(\frac{\partial^2 H}{\partial x^2}+\frac{\partial^2 H}{\partial y^2}\right)+S_h \tag{6}$$

$$S_h=\frac{\rho}{c_p}\frac{\partial(\Delta H)}{\partial t} \tag{7}$$

$$H=h+\Delta H \tag{8}$$

$$h=h_{ref}+\int_{T_{ref}}^{T}c_p\,dT \tag{9}$$

$$\Delta H=\beta L \tag{10}$$

$$\beta=\begin{cases}0 & (T<T_s)\\ 1 & (T>T_L)\\ (T-T_s)/(T_L-T_s) & (T_s<T<T_L)\end{cases} \tag{11}$$

初始条件：

$t=0$，$u=v=0$，$T_m=340$ K

边界条件：

$x=0$，$T=373.15$ K；$x=20$ mm，$\frac{\partial T}{\partial x}=0$；

$y=20$ mm，$y=0$，$\frac{\partial T}{\partial x}=0$

2　计算结果及分析

2 1　网格验证

网格质量直接关系到分析结果的准确性, 因此, 在数值计算之前, 有必要对网格进行验证。本研究按文献 [11] 建立物理模型进行验证。考虑到物理模型很规则, 故采用四边形网格, 该模型共产生 17 531个节点, 单元总数为 16 000. 经过计算比较, 再增大网格数得到的计算结果基本相同。

2 2　模型可靠性验证

为了验证所采用的数值模拟方法及模型的正确性, 按文献 [11] 的实验条件 (石蜡在热媒温度为 65 ℃时的光滑管内熔化) 下进行了模拟计算。图 3为该条件下内管距 32 mm处温度随时间的变化曲线, 通过对比数值模拟结果与文献 [10] 的实验结果, 发现二者吻合良好。

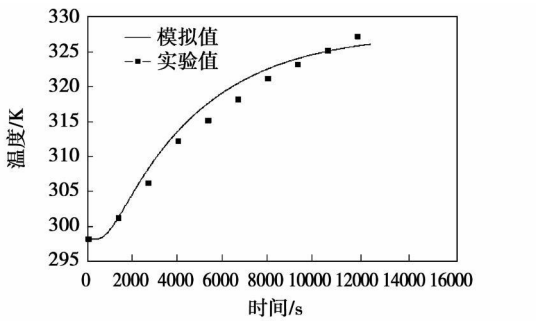

图 3　模拟值与实验值的比较[10]

2 3　石蜡熔化过程温度分析

为了研究石蜡熔化过程中温度随时间的变化情况, 数值模拟前设置了 3个监控点, 分别为 A(10 mm, 5 mm)、B(10 mm, 10 mm)、C(10 mm, 15 mm)。图 4是石蜡熔化过程中各点温度随时间变化曲线图。从图中可以看出: (1) 起始阶段, 矩形腔内石蜡的传热以导热为主, A、B、C点温度相差不大, 温度均随着时间推进按一定比率增大; (2) 200 s左右后, 石蜡开始逐步熔化, 发生相变, 由于相变储热, 温升速率有所减少, 曲线变得平坦; (3) 一段时间后, 由于熔化的液相石蜡密度小于固态石蜡, 在重力场作用下产生浮升力, 引起自然对流, 传热过程中自然对流逐步起主要作用。尽管传热温差逐步变小, 但各监控点温升速率开始加快, 液相石蜡开始向上部流动, 所以, 处于上半部分空间的 C点升温速率最快, 其次是处于中部位置的 B点, 再次是处于下半部分的 A点; (4) 熔化后期, 各监控点温度达到相变终点温度后, 温升速率有所减小, 这是由于液相石蜡导热系数低于固相石蜡, 且由于传热温差随熔化的不断进行而减小, 由此引起的自然对流作用提高不大。

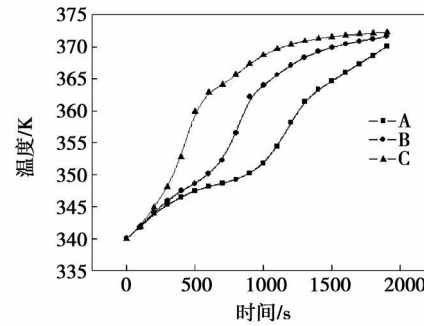

图 4　石蜡熔化过程中各点温度随时间变化图

2 4　石蜡熔化过程流场分析

图 5中表示了石蜡熔化过程中 =200、=500、t =800、=1 100 s时刻的流线图。由图中可以看出: 熔化初始阶段, 自然对流只发生在加热面附近, 且集中在左上角。这是由于左侧加热面的加热, 左侧石蜡最先熔化, 随后由于浮升力作用, 液相石蜡开始向上部流动。随着时间推进, 自然对流加强, 流线开始向右下部分推进, 自然对流的涡旋中心也随之移动并扩大, 直至熔解完成。

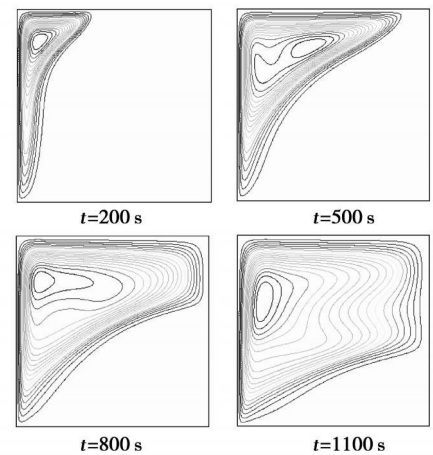

图 5　石蜡熔化过程中各时刻流线图

2 5　石蜡熔化过程相变界面分析

图 6表示石蜡熔化过程中 =200、=500、=800、=1 100 s时刻液相分数云图, 蓝色部分代表固相石蜡, 红色部分表示液相石蜡, 绿色部是石蜡两相区。左侧加热面的加热, 使导热由左侧向右侧推

进，由于热阻作用，矩形腔右侧石蜡导热较慢，而左侧加热面附近在 $t=200$ s时就有部分液相石蜡出现；由于自然对流作用，相界面并不是竖直的，而是向右下部分倾斜，随时间的推移，两相之间界面逐步向右下方移动，且两相区域的宽度有所增大。熔化末期，相界面弯曲接近于水平状态，但又稍有波动起伏。

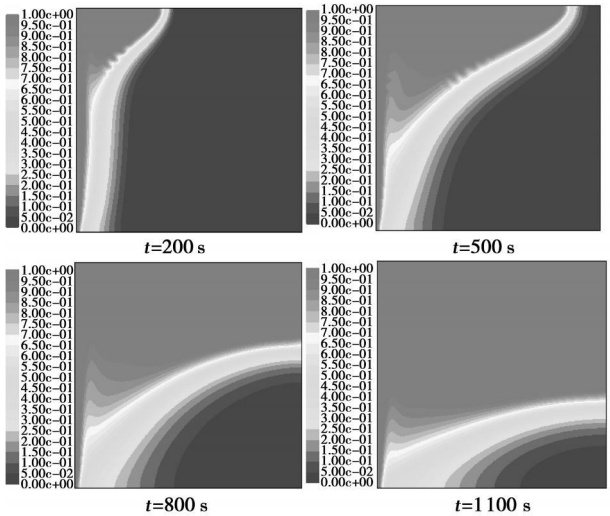

图 6 石蜡熔化过程中各时刻液相分数云图

2.6 翅片位置对石蜡熔化速率的影响

图 7为石蜡及加翅片后石蜡液相分数随时间的变化图。由图可以看出：(1)随着时间的推移，石蜡液相分数开始增大，翅片位置在 $y=5$ mm时，液相分数增加得最快。这是由于石蜡在熔化过程中，相界面逐步向右下部分推移，热阻主要集中在右下部分。该位置加翅片后，能在翅片表面上下区域双向强化大热阻区域的传热，形成自然对流；(2)熔化前期，翅片处于中间位置（$y=10$ mm)时石蜡液相分数增加速率要大于翅片处于底部位置（$y=0.1$ mm)，这是由于中间位置翅片能在翅片上下两表面都能起到强化传热作用，而处于底部位置的翅片只是在其上表面起到强化传热作用。但是由于热阻主要集中在矩形腔体下半部分，翅片处于中间位置时，强化传热作用随着时间推移逐步弱化，而翅片在底部位置（$y=0.1$ mm)时强化传热作用仍较强，所以最终熔化时间比翅片在中部位置（$y=5$ mm)时要短 (翅片在各位置下最终熔化时间如表 2所示)；(3)翅片对石蜡强化传热作用明显，它不仅提供了附加的热传导路径，而且促进了相变材料熔解区内的自然对流。在 $y=0.1$、$y=5$、$y=10$、$y=15$ mm时，储热时间分别缩短了 43.1%、52.0%、38.3%、22.2%。翅片位置与熔化时间的拟合函数如图 8所示。

表 2 翅片位置对石蜡熔化时间的影响

翅片位置 /mm	熔化时间 / s
$y=0.1$	1 030
$y=5$	869
$y=10$	1 117
$y=15$	1 408
无翅片	1 810

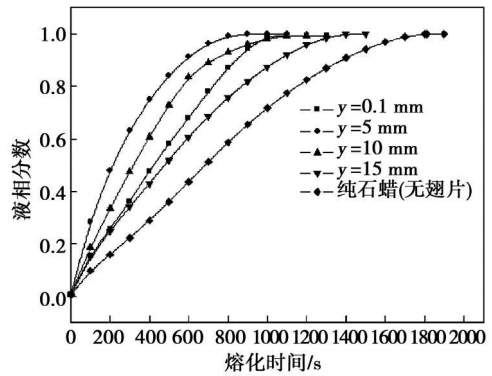

图 7 翅片位置对石蜡熔化速率的影响

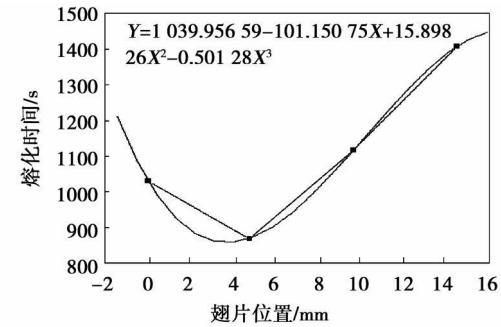

图 8 翅片位置对石蜡熔化时间影响

3 结 论

选取了一种适合利用 100 ℃左右蒸汽及烟气余热的相变材料，石蜡在熔化储热过程中，导热系数较小导致了石蜡与传热流体之间的大热阻，减小了传热速率，降低了蓄热器的性能。因此，通过矩形腔体内石蜡熔化过程及 4个位置下翅片对石蜡的强化传热的数值模拟，得出以下结论：

(1)石蜡熔化时，相界面随着时间推进向右下部分推移，矩形腔体内石蜡热阻主要集中在右下部分。

(2)翅片对石蜡强化传热作用明显,在 $y=0.1$、$y=5$、$y=10$、$y=15$ mm时,储热时间分别缩短了 43.1%、52.0%、38.3%、22.2%,在 $y=5$ mm处加翅片对石蜡强化传热作用最为明显。

(3)石蜡熔化过程中各点温升速率不同,但基本上要经历 4个阶段:(a)导热过程。石蜡在传热温差下温度快速升高;(b)相变过程。由于相变储热,温升速率有所减缓;(c)自然对流强化传热过程。相变完成后,由于自然对流强化传热,温升速率加快;(d)传热减弱过程。熔化后期,由于温差减小,自然对流提高不大,但液相导热系数小于固相,温升速率随时间推移逐渐减小。

参考文献:

[1] 抚顺石油研究院. 石蜡[M]. 抚顺:石油研究院出版社, 1987.

[2] 郭茶秀,张务军,魏新利,等. 板式石蜡储热器传热的数值模拟[J]. 能源技术, 2006, 27(6): 243-248.

[3] 王　俊. 石蜡熔化蓄热的实验和理论研究[D]. 西安:西安交通大学, 2002.

[4] GUO CHAXIU, ZHANG WUJUN. Numerical simulation and parametric study on new type of high temperature latent heat thermal energy storage system[J]. Energy Conversion & Manage, 2008, 49: 919-927.

[5] KHODADADI J M, HOSSEINIZADEH S F. Nanoparticle-enhanced phase change materials (NEPCM) with great potential for improved thermal energy storage[J]. Heat and Mass Transfer, 2007, 34: 534-543.

[6] 王剑锋,陈光明,陈国邦,等. 组合相变材料储热系统的储热速率研究[J]. 太阳能学报, 2000, 21(3): 258-263.

[7] 肖　睿,何世辉,黄　冲,等. 四丁基溴化铵包络化合物在铜管内的对流传热特性[J]. 化工学报, 2007, 58(9): 2206-2210.

[8] XIAO RUI, WU SHUSHENG, FENG ZIPING. Experimental investigation of the pressure-drop of clathrate hydrate slurry (CHS) flow of tetra butyl ammonium bromide (TBAB) in straight pipe// Proc 10th Inter Conf on Thermal Energy Storage[C]. NJ USA, 2006: 153-161.

[9] 巫术胜,肖　睿,黄　冲,等. 四丁基溴化铵水合物在空调蓄冷中的应用研究[J]. 制冷学报, 2006, (27)6: 48-51.

[10] 邹得球,宋文吉,肖　睿,等. 石蜡乳状液储热技术研究进展与应用前景[J]. 现代化工, 2008, 28(7): 12-15.

[11] 张月莲,郑丹星. 石蜡相变材料在同心环隙管内的基本传热行为[J]. 北京化工大学学报, 2006, 33(2): 5-10.

(本文责任编辑　单丽华)

新技术、新工艺

高压除氧器金属应力状态和工作特性分析

《Теплоэнергетика》2009年 2月号分析了高压除氧器运行中易损伤的原因。介绍了除氧器在最受力区域内壳体应力状态计算和试验研究的结果,以及 $C_T3_{сп}$、$C_T3_{кп}$ 号碳素钢在不同状态下工作性能研究的结果。

高压除氧器在运行时易受损坏的壳体段是除氧器转接管接头与储气槽连接区域和加强肋到储气槽的焊接区域。

除氧器与储气槽连接区域内的最大应力达到 240~250 MPa,在刚性肋到储气槽的焊接区域内的最大应力为 130~180 MPa。

$C_T3_{сп}$ 和 $C_T3_{кп}$ 号钢的循环和腐蚀—循环耐裂性差别不大。长期热变形时效不会明显影响 $C_T3_{кп}$ 号钢的腐蚀—循环耐裂性;该特性保护指标不低于 $C_T3_{сп}$ 号钢的值。

计算表明,除氧器壳体按照低循环疲劳条件(即按照在最受力区域内产生裂纹的条件)的寿命约为 45年。腐蚀—疲劳裂纹发展阶段寿命计算证明,按照腐蚀疲劳的机理,裂纹可能从它们约 3 mm深度开始加速增长,并且在最受力区域的金属的目视检查时能保证除氧器无故障工作的时间不少于 6年。

(吉桂明　摘译)

With the energy-saving modification of a high-pressure water return flow system cooled by Baogang N, steelmaking coal-gas and automatic return flow device performance testing system serving as the objects of study, through analysis of the dynamic characteristics of the automatic return flow valve group of the high-pressure water circulating control system, it has been verified that the device combines a variety of control functions such as flow rate induction, non-return, bypass control and multi-stage pressure reduction etc. into an integrated whole. This makes it possible to rationally simplify the complicated bypass return flow system and achieve a slow and smooth regulation. As a result, the normal operation flow path of the pumps is effectively guaranteeed, avoiding a fluid evacuation at a large flow rate and securing the aim of energy-saving and safe operation. It has been proven by an analysis of the dynamic characteristics of the high pressure water supply system and the practical application in several energy-saving modification projects that the valve group in question has fully met various technical and economic performance indexes required by the design and on-site operation technological process. Key words: coal gas cooling; high pressure water; automatic return flow valve group; dynamic testing; self-force driving; control cycle

中间再热机组一次调频特性研究 = Study of the Primary Frequency-modulation Characteristics of an Intermediate Reheat Unit[刊, 汉] / MA Su-xia(College of Electrical and Power Engineering, Taiyuan University of Science and Technology, Taiyuan, China, Post Code: 030024), MA Qing-zhong, ZHANG Long-ying (Shanxi Provincial Electric Power Corp., Academy of Electric Power Sciences, Taiyuan, China, Post Code: 030001) // Journal of Engineering for Thermal Energy & Power. — 2010, 25(1). —72 ~76

In the light of the great change in power grid frequency and the poor performance of primary frequency-modulation of the on-line units, the regulating system of an intermediate reheat steam turbine unit was redesigned to superimpose the frequency difference signal to the instructions for HP and IP regulating valve in the form of a feedforward signal to let the HP (High Pressure) and IP (Intermediate Pressure) regulating valve take part in the primary frequency modulation simultaneously. This makes it possible to fully use the heat stored in the intermediate reheat volume. The simulation results show that after the feedforward signals have been provided for the HP and IP regulating valve, the primary frequency modulation performance of the reheat steam turbine unit has been greatly improved with the load response ability being enhanced remarkably, retaining at the same time the stable performance of the regulation system. However, to realize feedforward signal control mode of the IP regulating valve still necessitates the completion of relevant research. Key words: primary frequency modulation; high pressure regulating valve feedforward; intermediate pressure regulating valve feedforward; intermediate reheat unit

一种余热利用相变石蜡储热过程的数值模拟 = Numerical Simulation of the Heat Storage Process of a Waste Heat Utilization-oriented Phase-change Paraffin[刊, 汉] / ZOU De-qiu(Postgraduate School, Chinese Academy of Sciences, Beijing, China, Post Code: 100039), XIAO Rui, SONG Wen-ji, FENG Zi-ping(Key Laboratory on Renewable Energy and Natural Gas Hydrate, Guangzhou Energy Source Research Institute, Chinese Academy of Sciences, Guangzhou, China, Post Code: 510640) // Journal of Engineering for Thermal Energy & Power. — 2010, 25(1). —77 ~81

Based on a kind of phase-change heat storage paraffin and with its liquid phase natural convection during its melting process being taken into consideration, a mathematical model for the paraffin melting process inside a rectangular cavity was established and used to perform a numerical simulation. In addition, the change of the temperature and flow field and the shift of the interphase boundary during the paraffin melting process was analyzed. The heat transfer was intensified by utilizing an aluminium-made fins and the influence of the fin location on the paraffin melting time was also analyzed. The simulation results show that when the location of the fins y=0.1 mm, y=5 mm, y=10 mm and y=15 mm, the heat storage time was shortened by 43.1%, 52.0%, 38.3% and 22.2% respectively as compared with the case when the fins are not used. The research results are of definite significance to

the optimized design of a phase-change heat accumulator. Key words: paraffin, phase change, intensified heat transfer, numerical simulation, waste heat utilization

石灰立窑代焦型煤燃烧特性的实验研究 = Experimental Study of the Combustion Characteristics of Briquette as a Substitute for Coke in a Vertical Lime Kiln[刊, 汉] / PENG Hao-yi, LIU Yan-jun, ZHOU Jie-min (College of Energy Science and Engineering, Central South University, Changsha, China, Post Code: 410083) // Journal of Engineering for Thermal Energy & Power. — 2010, 25(1). 82~86

On a SDTQ600 type temperature-difference-thermogravimetric combined analyzer, a thermogravimetric analysis was performed of the briquette sample which substituted the coke in a vertical lime kiln, and the influence of the different temperature rising speeds on its combustion characteristics was studied. In the meantime, the briquette, coke and anthracite block coal sample were compared with each other at a temperature rising speed of 5 ℃/min. The combustion rate of a single particle of the briquette was investigated by employing a muffle furnace. It has been found that the briquette coal combustion process experiences four stages, i.e. drying and preheating, volatile element precipitation, carbon particle combustion and carbon residue burn-out. With an increase of the temperature rising speed, the reaction time required by various combustion stages of the briquette was shortened and the reaction rate was speeded up. When the temperature rising speed increases from 5 ℃/min to 10 ℃/min and 15 ℃/min, the briquette ignition time will be shortened from 28.12 min to 14.01 min and 10.13 min while the burn-out time will also be reduced from 36.82 min to 27.59 min and 22.47 min. Through a contrast, the briquette is the best in terms of the ignition, stable combustion performance and comprehensive combustion characteristics while the burn-out performance ranks at the middle place. The comprehensive combustion indexes of briquette, coke and anthracite block coal representing three kinds of sample are 53.25×10^{-9}, 30.14×10^{-9} and 11.53×10^{-9} respectively. The combustion temperature exercises a relatively small influence on the combustion speed of the briquette while the briquette size has a relatively conspicuous impact on the combustion speed at the later stage. To reduce the size of the briquette can increase its combustion speed. Under the same conditions, the combustion speed of the briquette is lower than that of coke but higher than that of anthracite block coal. The test results can offer guidance for the briquette as a substitute for coke in vertical lime kiln. Key words: briquette as a substitute for coke, combustion characteristics, thermogravimetric analysis, combustion rate, vertical lime kiln

NH_3选择性非催化还原NO的实验研究 = Experimental Study of Selective Non-catalytic Reduction of NO by NH_3[刊, 汉] / CAO Qing-xi, WU Shao-hua, LIU Hui, et al (College of Energy Science and Engineering, Harbin Institute of Technology, Harbin, China, Post Code: 150001) // Journal of Engineering for Thermal Energy & Power. — 2010, 25(1). —87~90

On an electrically-heated tubular reaction stove, an experimental study was performed of a gas phase homogeneous reaction of NH_3 to selectively and non-catalytically reduce NO. The test results show that the optimum denitration temperature is around 925 ℃ with the maximum denitration efficiency being 83%. With the denitration efficiency, NH_3 leakage loss and operation cost being taken into account as a whole, the optimum ammonia mol ratio is 1.5. When the initial concentration of NO decreases from 300 μL/L to 100 μL/L, the denitration efficiency will go down from 83% to 57%. The NOx emissions concentration after the denitration, however, is about 50 μL/L, almost without any changes. When the oxygen concentration increases from 1% to 10%, the denitration efficiency will decline from 91% to 75% and the remaining NH_3 after the reaction will diminish from 43 μL/L to 10 μL/L. At 925 ℃, to complete a SNCR (selective non-catalytic reduction) reaction process will require more than 1 second of residence time, while at 1 000 ℃, the process will need only 0.4 seconds. Key words: selective non-catalytic reduction, denitration efficiency, ammonia and nitrogen ratio, ammonia leakage loss